

# Deviations From the Random Plane Wave Field Distribution in Electromagnetic Enclosures

Farasatul Adnan , Steven M. Anlage , *Member, IEEE*, Thomas M. Antonsen Jr., *Life Fellow, IEEE*, and Edward Ott, *Life Fellow, IEEE*

**Abstract**—Wave energy distribution within enclosures with irregular boundaries is a common phenomenon in many branches of electromagnetics. If the wavelength of the injected wave is small compared with the structure size, the scattering properties of the enclosure will be extremely sensitive to small changes in geometry or wave frequency. In this case, statistical models are sought. The random coupling model (RCM) is one such model that has been explored through experiments and theory. Previous studies were conducted by injecting waves into high Q cavities in a nearly omnidirectional manner. In this article, a directed beam approach is taken, and relatively low Q cavities are considered. The goal is to determine when the so-called “random plane wave hypothesis,” a fundamental basis of the RCM formulation, breaks down. Results show that injecting such directed beams leads to large deviations in the wave statistics for single realizations of the enclosure geometry. The expected statistics are restored to some degree when multiple realizations are considered.

**Index Terms**—Electromagnetic compatibility (EMC), overmoded cavities, radiation impedance, ray chaos, statistical electromagnetism, wave chaos, wave scattering.

## I. INTRODUCTION

ELECTROMAGNETIC (EM) coupling within systems of enclosures that are connected by apertures or ports is an important problem for the EM community that regularly appears in various forms. Examples include EM compatibility studies for electronic components under high-power microwave exposure [1], [2], wireless signal propagation inside rooms or buildings [3], and even coupled quantum mechanical systems modeled with superconducting microwave billiards [4].

For most irregular geometries, an analytical solution for the wave fields does not exist. In these cases, one can numerically

solve the governing Maxwell’s equations using methods such as the finite-element method [5] or the finite-difference time-domain [6] method. Although these numerical approaches are powerful, they can be time-consuming to implement in the case of high-frequency applications due to the need for a fine mesh. In the small wavelength limit, where the ratio of the enclosure dimensions to the wavelength is large, the numerical solver must mesh the geometry covering it with a very large number of grid points. The amount of memory and computational power required to numerically solve these problems can thus become impractical. Furthermore, such deterministic solutions of these complicated geometries often depend sensitively on details (such as the exact shape of the boundary; the position, shape, and number of scatterers; or the exact location and shape of the injecting ports) of the system that may not be known. Even if the details are known, the nature of the waves in the complex enclosures is such that a small change in the boundary conditions or the frequency dramatically changes the wave fields, thereby changing the solution substantially [7], [8], [9].

To study wave coupling in the small wavelength limit, researchers frequently resort to approximate solutions of the governing equations that are simpler to implement. Rather than solving such systems exactly, it is often desirable to create statistical models. Then, one can describe the general properties of such systems without the need for accurately modeling the details. One successful statistical approach to describing wave dynamics in such cases is known as the random coupling model (RCM) [10], [11], [12], [13], [14], and it is based on a combination of the random matrix theory (RMT) [15] and the random plane wave hypothesis [16], [17], [18], [19], [20].

The RCM provides a statistical model for the impedance matrix that describes the linear relation among the currents and voltages at specified ports. The relevant properties of the ports needed for the model are the port radiation impedances. These are the first approximations of the impedance values the ports would have if there were no enclosure and the ports radiated into free space. The basic RCM also includes information about the enclosure, in particular the ratio of the decay rate of fields due to losses and the average spacing in frequency between modes of the enclosure. The distribution of resonant mode frequencies is given by RMT. A key assumption in the use of the basic RCM is that the mode fields at any point in the enclosure are well approximated by a random superposition of plane waves with uniformly distributed directions and phases.

Manuscript received 3 July 2022; revised 12 November 2022; accepted 6 December 2022. Date of publication 29 March 2023; date of current version 14 April 2023. This work was supported in part by AFOSR/AFRL under Grant FA9550-15-1-0171, in part by ONR under Grant N000141912481, and in part by DARPA under Grant HR00112120021. (*Corresponding author: Farasatul Adnan.*)

Farasatul Adnan is with the Qorvo Inc., Apopka, FL 32703 USA (e-mail: faradnan@gmail.com).

Steven M. Anlage is with the Department of Physics, the Department of Electrical and Computer Engineering, and the Quantum Materials Center, University of Maryland, College Park, MD 20742 USA (e-mail: anlage@umd.edu).

Thomas M. Antonsen and Edward Ott are with the Department of Physics, the Department of Electrical and Computer Engineering, and the Institute for Research in Electronics and Applied Physics, University of Maryland, College Park, MD 20742 USA (e-mail: antonsen@umd.edu; edott@umd.edu).

Color versions of one or more figures in this article are available at <https://doi.org/10.1109/TEMC.2023.3235824>.

Digital Object Identifier 10.1109/TEMC.2023.3235824

The RCM has been thoroughly tested both in experimental and simulation/numerical settings. It was found that systematic deviations from RCM statistical predictions appeared if data from a too narrow range of frequencies were considered. These deviations were traced to a breakdown in the so-called random plane wave hypothesis, where in a suitable approximate sense, the fields within the cavity behave as a random superposition of isotropically propagating plane waves [14], [15], [16], [17]. The breakdown was associated with the presence of relatively short ray paths from the transmitting port to the receiving port. The effect of these paths can be eliminated if statistics are collected over a range of frequencies larger than the reciprocal of the travel time for a ray along the path, or if the properties of the path are known, they can be incorporated in the port impedances [21], [22].

Since the deviations from the basic RCM model are associated with the presence of short ray paths connecting ports, it is interesting to ask: What is the role of the directivity of the radiating structures that constitute the ports? On the one hand, the effect of a ray path will be enhanced if the ray leaves the transmitting port or arrives at the receiving port along a direction where the gain profile of the port is high. On the other hand, the contributions from ray paths that start or end along directions of low gain can be expected to decrease. In this article, we show that by injecting waves in a directed manner, one can cause the values of the scattering matrix elements to deviate from the RCM predictions. In other words, one can *break* the RCM model by injecting waves in a more directed manner. This has two important consequences. First, it invalidates, in some circumstances, the estimates for field strengths in irradiated enclosures. The true values will tend to be larger than the estimates. Second, it opens up new avenues for research in the RCM where port directivity can be incorporated as a parameter in the relevant formulations.

We will find that the deviations depend in a complicated way on a number of factors: the directivity of the ports, the frequency of the radiation, and the energy loss rate for the cavity. Roughly speaking, deviations are largest in cases where the ports are highly directive, either due to their geometry or due to their frequency of operation, and the damping is strong enough that a ray will be absorbed before it can bounce around in the cavity and contribute to a random superposition of waves.

This article is organized as follows. In Section II, we briefly review the RCM. In Section III, we briefly review the short-orbit effect. In Section IV, we present simulation results that show the deviations from the RCM predictions due to the injection of a directed beam of waves within a chaotic enclosure. Also, we compare these results to those of a simulation in which waves are injected isotropically. Finally, Section V concludes this article and discusses future work.

## II. RANDOM COUPLING MODEL

The RCM is a statistical model used to characterize the impedance matrix of a multiport, complex, overmoded EM cavity. It is based on a combination of the random plane wave approximation, in which the fields at any point in the enclosure consist of the random superposition of isotropically propagating

plane waves with random phases, and RMT, which provides the statistical distributions.

The main result from the RCM is that the cavity impedance,  $Z$ , at a single port in a wave chaotic cavity is given in terms of system-specific deterministic quantities and a universally distributed random quantity [11], expressed in the following formula:

$$Z = jX_{\text{rad}} + \xi R_{\text{rad}} \quad (1)$$

where  $R_{\text{rad}}$  and  $X_{\text{rad}}$ , respectively, are the real and imaginary parts of the radiation impedance  $Z_{\text{rad}}$ , which is the impedance of the port excluding contributions from the cavity. In other words,  $Z_{\text{rad}}$  is the impedance that would be measured if the cavity walls were moved out to infinity. The quantity  $\xi$  is a complex random variable [14] whose probability distribution is fully characterized by a single loss parameter  $\alpha$ . It is defined as follows:

$$\xi = -\frac{j}{\pi} \sum_n \frac{\Delta k^2 \phi_n \phi_n^T}{k^2 - k_n^2 + j\alpha \Delta k^2} \quad (2)$$

where  $\phi_n$  is a vector of independent and identically distributed, zero-mean, unit-variance Gaussian random variables. The series  $k_n^2$  represents the squares of the eigen-wavenumbers of the normal modes of the closed system. These are taken to be random variables whose normalized distribution is described by RMT [15]. The quantity  $\alpha$  is the loss parameter, and  $\Delta k^2 = \langle k_{n+1}^2 - k_n^2 \rangle$  is the mean mode spacing. The loss parameter  $\alpha$  characterizes the loss in the enclosure; it is essentially the average  $Q$ -width of resonant modes in the cavity normalized to the average spacing between modes. Also,  $\alpha$  can be evaluated as  $\alpha = k^2 / (Q \Delta k^2)$ , where  $k$  is the wave number of interest and  $Q$  is the quality factor [14].

From this point on, we focus on quasi-2D cavities because they are more easily simulated and analyzed. By quasi-2D, we mean cavities that have very small heights compared with their lengths and widths. Such cavities support a set of modes with frequencies below a cut-off for which the height is half a vacuum wavelength. The electric field for such modes is directed parallel to the height, and the magnetic field is transverse to the electric field. Both fields have insignificant variations along the direction of the height of the cavity. By considering these modes, we eliminate the effects of wave polarization, which is a further simplification. We expect that the basic phenomena uncovered by considering quasi-2D cavities will also be revealed in 3-D cavities. We defer verification of this to future work.

Returning to the evaluation of (2), we note that according to Weyl's formula [23] for a 2-D cavity of area  $A$ , the mean spacing between two adjacent squared eigen-wavenumbers is given by  $\Delta k^2 = 4\pi/A$ . Furthermore, a method to generate an ensemble of  $k_n^2$  to be used in (2) is described in [24, Appendix].

The impedance formula (2) can be extended to a multiport cavity [12] as follows:

$$Z = jX_{\text{rad}} + R_{\text{rad}}^{1/2} \xi R_{\text{rad}}^{1/2} \quad (3)$$

where all the variables are now matrices. Therefore, the matrix  $Z_{\text{rad}}$ , mean mode spacing, and loss parameter  $\alpha$  are the system-specific quantities necessary to apply the RCM, which

then allows us to predict the statistics of the impedance of a chaotic cavity.

### III. SHORT-ORBIT EFFECT

Previous comparisons of experimental data with RCM predictions have often employed ensembles of realizations of the system to compile statistics. To create such ensembles, researchers have typically varied the geometrical configuration of the scattering region and/or taken measurements at different frequencies [21], [22]. These variations are intended to create a set of systems in which the properties of the ports and the loss factor are preserved, but the detailed field patterns are varied. Thus, by suitably accounting for the port details, it was hoped that only universal properties remained in the ensemble data. However, there can be problems in practice. For example, in the case of geometrical configuration variation, researchers typically move perturbing objects inside a ray-chaotic enclosure with a fixed shape and size or move one wall of that enclosure to create an ensemble of systems with varying details. The problem is that certain walls or other scattering objects of the enclosure remain fixed throughout the ensemble. Therefore, there may exist relevant ray trajectories that remain unchanged in many or all realizations of the ensemble. We term such ray trajectories that leave a port and soon return to it (or another port) before ergodically sampling the enclosure “short ray trajectories” or “short orbits.”

A “short orbit” refers to a ray trajectory whose length is not much longer than several times the characteristic size of the EM enclosure. This type of trajectory is shown in a 2-D cavity in Fig. 1, as reproduced from [25]. The circular scatterer is a movable object for creating different boundary realizations and is used to create an ensemble. However, in the case of geometries such as those in Fig. 1, the effect of the short orbit persists in many realizations, being eliminated only if blocked by the scatterer.

Generally, the length of the orbits that are of interest is determined by the range of frequencies over which the window average of the impedance is desired. For example, if the window average is made with a Lorentzian kernel of width  $\Delta\omega$ , the average is equivalent to evaluating the exact impedance at a complex frequency  $\omega - j\Delta\omega$ . The effect of orbits corresponding to travel times longer than  $T = 1/\Delta\omega$  is eliminated by frequency window averaging. This idea of short orbits is important for this work, as we expect the highly directive source in combination with short orbits to cause deviations from the RCM predictions. However, it is important to point out that previous researchers have carried out “Short-Orbit Corrections” to the RCM, which can lead to improved predictions of the RCM even when short orbits are present [21], [22].

### IV. INJECTING DIRECTED BEAMS IN A CHAOTIC CAVITY

The goal of this article is to report an investigation of whether the RCM is applicable if a highly directed beam is used to inject energy into a chaotic cavity. Previous RCM studies in 2-D have utilized a source that radiates isotropically. Here, we consider the effect of a source with a directed beam.

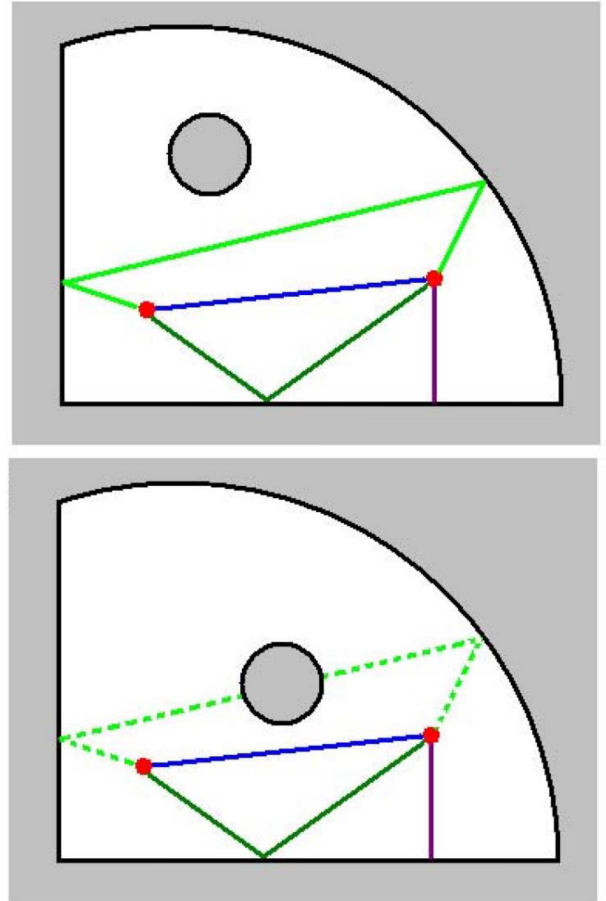


Fig. 1. Illustrations of short orbits in a 2-D cavity with a circular scatterer. The red dots are the ports, and the colored lines are examples of short orbits. The blue lines are direct orbits. The two-bounce orbit (light green) in the top figure is blocked in the bottom figure due to the shift of the scatterer. Figure reproduced from [25].

The basis for much of the previous work on RCM is “the random plane wave hypothesis” [16], [17], [18], [19], [20]. In short, this hypothesis states that the fields within the cavity behave like a random superposition of isotropically propagating plane waves. Therefore, the eigenfunctions  $\phi(\mathbf{X})$  of the Helmholtz equation can be approximated by a superposition of the plane waves with wavenumber  $k_n$  such that

$$\phi(\mathbf{X}) = \sum_{j=1}^N a_j \cos(ik_n \hat{e}_j \cdot \mathbf{X} + i\theta_j) \quad (4)$$

where  $a_j$  are independent and identically distributed random variables,  $\hat{e}_j$  is an independent isotropically distributed random unit vector,  $\theta_j$  is an independent and uniformly distributed random variable in  $[0, 2\pi)$ . The normalization of the amplitudes  $a_j$  is determined by the assumed normalization of the eigenfunctions and the number of amplitudes  $N$ ,  $\phi^2 = Na_j^2/2$ . The “ $\cdot$ ” in this equation refers to the dot operator between two vectors and  $i$  is equal to  $\sqrt{-1}$ .

The eigenfunctions can be thought of as a superposition of a large number  $N$  of plane waves. The coupling coefficients in the RCM are proportional to the port directivity averaged over the  $N$

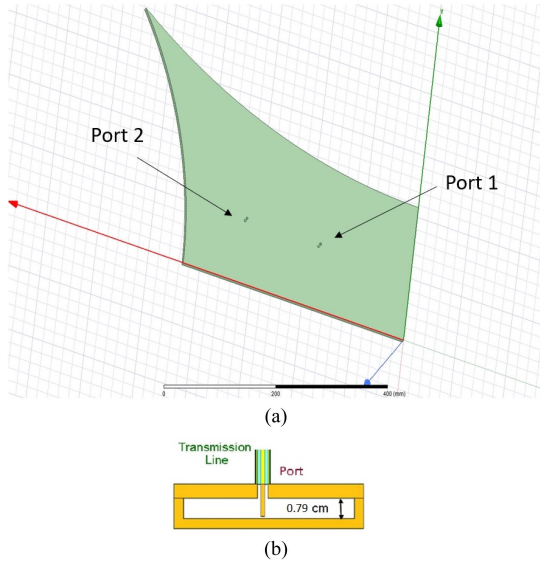


Fig. 2. (a) View of the quasi-2D bowtie cavity with coaxial sources created in HFSS. (b) Schematic diagram illustrating a cross-sectional view of the bowtie cavity through a port. Fig. (b) reproduced from [14].

plane waves. For large  $N$ , this becomes the average of the port directivity. However, there are fluctuations that scale as  $N^{-1/2}$ . If the port is highly directive, these fluctuations are enhanced. Furthermore, it is expected that such a directed beam would lead to enhanced short-orbit effects. Evidence for that prediction is also presented in this section.

To study the role of port directivity, we designed a chaotic bowtie-shaped cavity, as shown in Fig. 2(a), using the popular full-wave commercial solver ANSYS HFSS. The dimensions of the bowtie are the following: The lower and left straight sides of the cavity have lengths  $L_1 = 418$  cm and  $L_2 = 21.59$  cm, respectively, and the upper and right sides have radii of curvature  $R_1 = 103$  cm and  $R_2 = 63.9$  cm. The thickness of the cavity is 7.9 mm in the  $z$ -direction. We placed a circular scatterer in the cavity, which has a radius of 40 mm. This scatterer was placed in various positions inside the cavity to create a number of realizations. In all the simulations described in this article, the scatterer was kept fully reflective. We added losses to the straight and curved walls of the cavity, and the losses were then varied.

To compare ports with varying directivity, we designed two types of ports. The first type is omnidirectional. It consists of a coaxial cable with inner and outer conductors connected through the top plate of the cavity. Ports of this type are labeled Port 1 and Port 2 in Fig. 2(a). Port 1 is centered at location  $x = 18.03$  cm and  $y = 12.47$  cm, and Port 2 is at  $x = 32.43$  cm and  $y = 12.47$  cm. The distance between the ports is 15 cm. Both ports have an inner radius of 0.868 mm and an outer radius of 2 mm. The outer conductor touches the top plate of the bowtie, whereas the inner conductor extends inside the cavity as shown in Fig. 2(b), leaving a small gap (0.01 mm) between it and the bottom plate.

The second type of port used is an aperture in the side walls of the cavity. This is done to simulate ports with increased directivity of the EM wave energy that is entering the cavity.

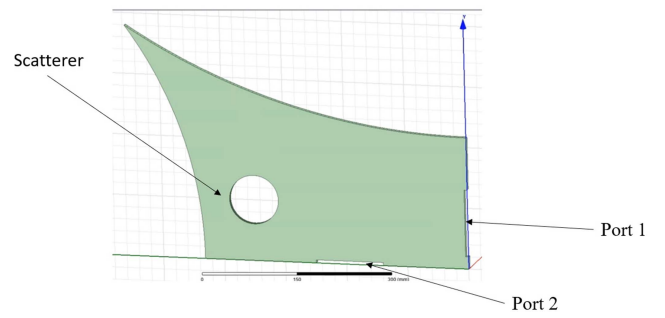


Fig. 3. View of the quasi-2D bowtie cavity with a circular scatterer created in HFSS.

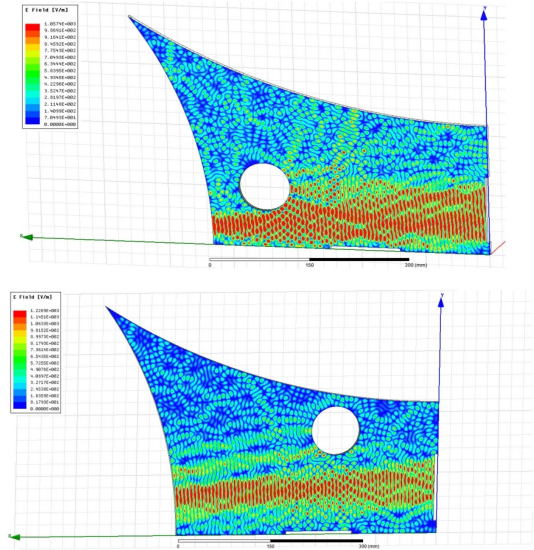


Fig. 4. View of the magnitude squared of the complex E-field in a quasi-2D bowtie cavity with a circular scatterer in different positions at 25 GHz for aperture-like ports. Blue represent the lowest intensity, and red represent the highest intensity. The walls have a loss of  $80 \Omega$  while the scatterer is perfectly reflective. At this frequency, the beam is very directive, as shown by the E-field plots.

Apertures of different sizes were considered. The apertures were treated in HFSS as single-mode wave ports. The largest apertures are 110 mm wide and are shown in Fig. 3. The directivity of an aperture port depends on the frequency and size of the aperture. Radiation is emitted from the aperture in a range of angles. If  $L_A$  is the size of the aperture, the radiated energy comes out in a wedge of angular width  $\Delta\theta \approx \lambda/(2L_A)$ . The directivity of the aperture port is evident in Fig. 4, where the magnitude of the electric field is plotted as a function of position in the cavity for two positions of the scatterer and excitation frequency is 25 GHz.

Fig. 5 shows the field profiles for the coaxial, isotropic ports. In these simulations, the walls of the bowtie have a surface resistance of  $80 \Omega$  while the scatterer is perfectly reflective. These field profiles are qualitatively different from the directed port case shown in Fig. 4. They are more evenly distributed across the cavity.

To compare the statistics of the fields under excitation by different port types, we excited the cavity over a range of

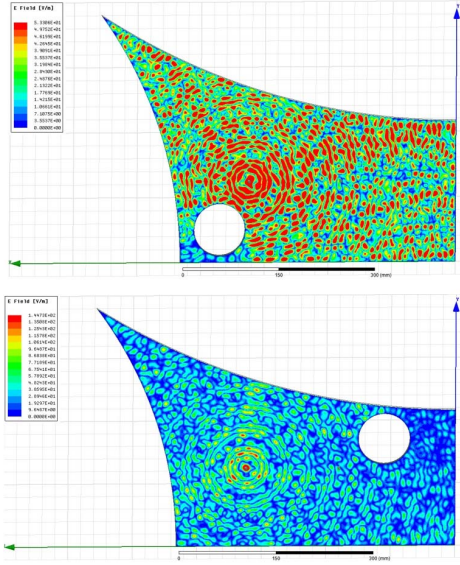


Fig. 5. View of the E-field in a quasi-2D bowtie cavity with a circular scatterer in different positions at 25 GHz for coaxial ports.

frequencies from 24 to 26 GHz and recorded the values of the elements of the  $2 \times 2$  impedance matrix. Six scatterer positions were used for each port type. We can then examine the statistics of the impedance matrices for a fixed scatterer position and an ensemble of frequencies, or for a total ensemble of both frequencies and scatterer positions. Figs. 6 and 7 show the real and imaginary parts of  $Z_{12}$  as functions of frequency for aperture ports and coaxial ports, respectively.  $Z_{12}$  here refers to the impedance seen between ports 1 and 2. Different colors represent different scatterer positions.

To compare the statistics of the impedance values, we have normalized them as follows. We introduce a scaled impedance matrix according to

$$\begin{bmatrix} \zeta_{11} & \zeta_{12} \\ \zeta_{21} & \zeta_{22} \end{bmatrix} = \begin{bmatrix} \frac{Z_{11} - \bar{Z}_{11}(\omega)}{R_{1,\text{rad}}} & \frac{Z_{12} - \bar{Z}_{12}(\omega)}{\sqrt{R_{1,\text{rad}} R_{2,\text{rad}}}} \\ \frac{Z_{21} - \bar{Z}_{21}(\omega)}{\sqrt{R_{1,\text{rad}} R_{2,\text{rad}}}} & \frac{Z_{22} - \bar{Z}_{22}(\omega)}{R_{2,\text{rad}}} \end{bmatrix}. \quad (5)$$

Here,  $\zeta_{nm}$  represents the normalized impedance, and  $Z_{ij}$  are various elements of the impedance matrix as generated by HFSS. The  $\bar{Z}_{ij}(\omega)$  quantity represents the average impedance, which is the mean taken over all the scatterer positions. The  $\bar{R}_{\text{rad}}$  quantities are defined in terms of the diagonal elements as  $\bar{R}_{1,\text{rad}} = \text{Re}\{\bar{Z}_{11}(\omega)\}$  and  $\bar{R}_{2,\text{rad}} = \text{Re}\{\bar{Z}_{22}(\omega)\}$ .

The averaging procedure was done as follows: We use a sliding window average for each of the six plots for  $Z_{12}$  versus frequency. The window frequency is taken to be 0.65 GHz. These ‘‘smoothed’’ results were then summed at each frequency and then divided by 6, the number of scatterer positions. These results were then averaged over frequencies. After this process,  $\bar{R}_{1,\text{rad}}$  is calculated as  $32.9 \Omega$  and  $\bar{R}_{2,\text{rad}}$  is  $33.7 \Omega$ . We had 200 data points from 24 to 26 GHz.

What can be seen by comparing Figs. 6 and 7 is that the graphs of impedance versus frequency for different scatterer positions in the case of the coaxial ports are similar, whereas the graphs

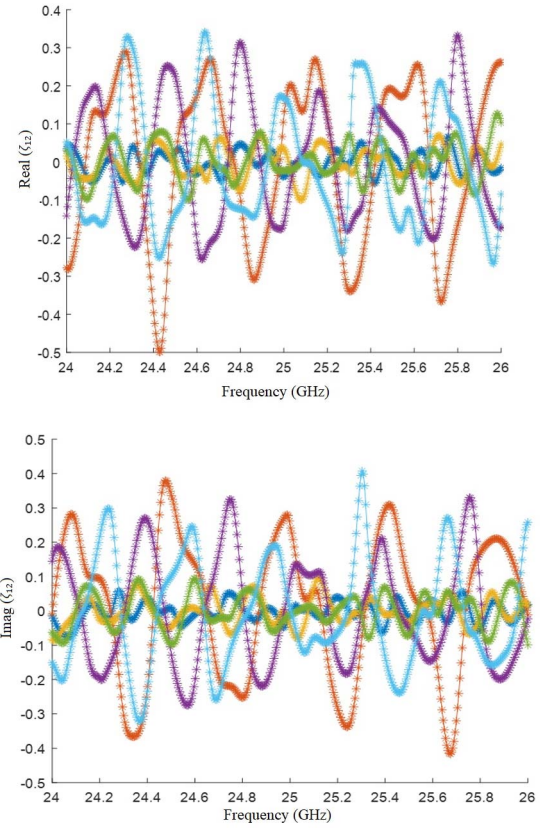


Fig. 6. Top and bottom: real and imaginary parts of various components of the Z matrix versus frequency for aperture-like ports. Different colors represent different scatterer positions. These results are normalized as described in (5). Wall loss is  $80 \Omega$ .

for different scatter positions in the case of the aperture ports differ from each other. In the aperture case in Fig. 6, three of the curves show consistently smaller impedance values than the other two. To further illustrate these deviations, we constructed histogram plots for the real part of the  $Z_{12}$  data for each scatterer position. These are shown as the solid bars in Figs. 8 and 9. We also combined the data from different scatterer positions and constructed a composite histogram for the total ensemble for each of the port types. These are shown as the red line histograms.

Figs. 8 and 9 clearly show that for a very directive beam, Fig. 8, the impedance values for a particular scatterer position are very different from the values for the ensemble of realizations. This is not the case for the isotropic ports, Fig. 9, where the histograms for individual realizations are close to those of the ensemble.

Two factors can combine to contribute to the large deviations in the aperture case. These are the directivity of the ports and the relatively high value of wall loss. With a surface impedance of  $80 \Omega$ , the power reflection coefficient averaged over incident angles is  $R = 0.85$ . Thus, power is effectively extracted from the radiation beam in several bounces from the walls, and the narrow radiation beam does not reach all regions of the cavity and all directions before it is absorbed. We lowered the loss to  $40 \Omega$ . This should lead to more scattering from the walls for the

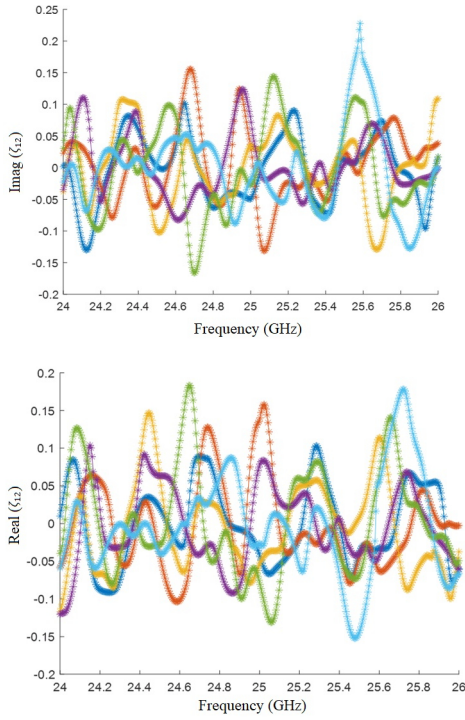


Fig. 7. Top and bottom: real and imaginary parts of various components of the  $Z$  matrix versus frequency for coaxial ports. Different colors represent different scatterer positions. These results are normalized as described in (5). Wall loss is  $80 \Omega$ .

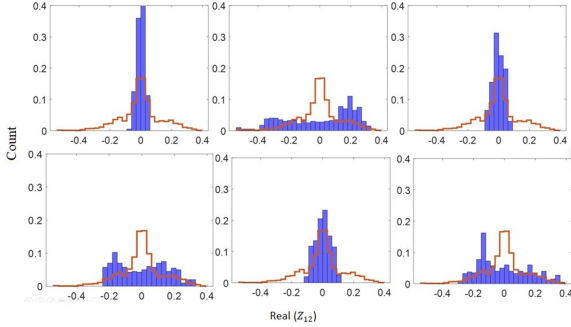


Fig. 8. Histogram plots for the normalized real ( $Z_{12}$ ) values (5) on the horizontal axes for six different scatterer positions. These histograms are for the 110-mm aperture-like sources at 24–26 GHz and  $80 \Omega$  wall loss. Blue bars show the real parts of  $Z_{12}$  for each scatterer position. The red staircase graph shows the histogram for the real values for all six scatterer positions combined.

EM waves, more ergodicity, and more uniformity realization. These results are plotted in Fig. 10.

Fig. 10 shows that lowering the loss has led to the individual histograms looking more similar to the ensemble (shown in red) than the case shown in Fig. 8. We then dropped the loss to  $10 \Omega$  on the wall, and these results are shown in Fig. 11.

Fig. 11 shows that the  $Z_{12}$  values for individual scatterer positions conform much more to those of the total ensemble. This may be understood as follows. For wave reflections from walls of surface impedances of 10, 40, and  $80 \Omega$ , the power reflection coefficients averaged over angle are 0.97, 0.91, and 0.85, respectively. Thus, for these surface impedances, a ray will bounce  $N_B = 39, 11,$  and 6 times before losing a fraction

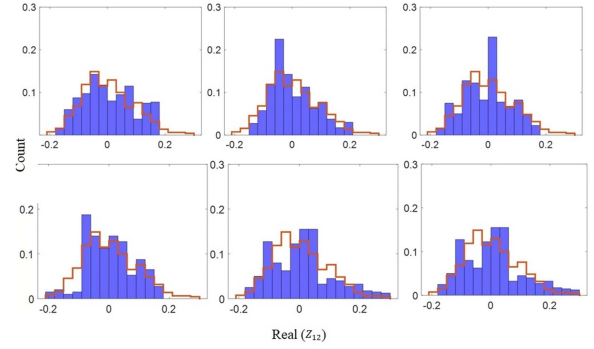


Fig. 9. Histogram plots for the normalized real ( $Z_{12}$ ) values (5) on the horizontal axes for different scatterer positions. These histograms are for the coaxial sources at 24–26 GHz and  $80 \Omega$  loss. Blue bars show the real parts of  $Z_{12}$  for a particular position. The red staircase graph shows the histogram for the real values for all six scatterer positions combined.

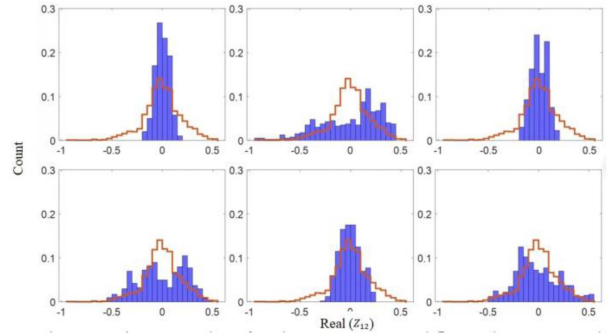


Fig. 10. Histogram plots for the normalized real ( $Z_{12}$ ) values (5) on the horizontal axes for six different scatterer positions. These histograms are for the 110-mm aperture-like sources at 24–26 GHz and  $40 \Omega$  loss. Blue bars show the real parts of  $Z_{12}$  for a particular position. The red staircase graph shows the histogram for the real values for all six scatterer positions combined.

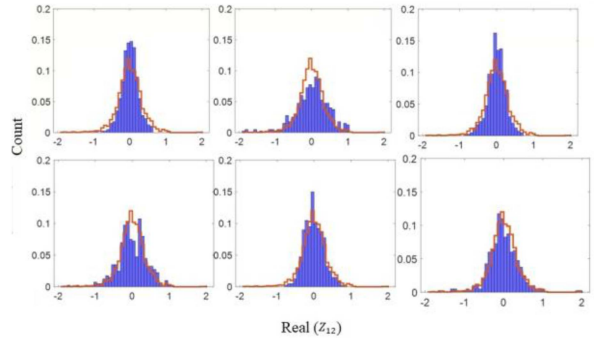


Fig. 11. Histogram plots for the normalized real ( $Z_{12}$ ) values (5) on the horizontal axes for six different scatterer positions. These histograms are for the 110-mm aperture-like sources at 24–26 GHz and  $10 \Omega$  loss. Blue bars show the real parts of  $Z_{12}$  for a particular position. The red staircase graph shows the histogram for the real values for all six scatterer positions combined.

(1- $e$ ) of its power. An aperture of  $L_A = 110$  mm radiates in the far field into a sector  $\Delta\theta \simeq \pi/(L_A k) = 0.054$  rad at 25 GHz. The far field result applies for distances greater than a Rayleigh length, which for the 110-mm aperture at 25 GHz is roughly 2 m. This corresponds to 5 bounces. Thus, we expect the radiation to be absorbed in the far field for the  $10 \Omega$  and  $40 \Omega$  surface impedance cases, but marginally for the  $80 \Omega$  case. If the cavity

TABLE I  
VARIANCE OF THE IMPEDANCE

$ij$	$v_{ij}$	$\mu_{ij}$ [80 $\Omega$ ]	$\mu_{ij}$ [40 $\Omega$ ]	$\mu_{ij}$ [10 $\Omega$ ]
11	1.0	2.44	2.35	1.82
12	0.5	0.65	0.68	0.57

were a square of side  $L$ , the extent of the illumination of the perimeter after  $N_B$  bounces would be  $L_E = N_B L \Delta\theta$ . Thus, a fraction  $f_E = N_B \Delta\theta / 4$  of the perimeter is irradiated after  $N_B$  bounces. For the three values of surface impedance, 10, 40, and 80  $\Omega$ , this fraction is  $f_E = 0.53, 0.15,$  and  $0.08$ . Thus, one can expect that for 10  $\Omega$  surface impedance, the random plane wave approximation and the RCM treatment of the cavity for a single position of the scatterer will become valid. One would not expect the RCM to be valid for the 40 or 80  $\Omega$  surface impedances. This is basically confirmed by comparing Figs. 8, 10, and 11.

The next issue we address is whether the composite histograms, the ones that combine data from six different scatterer positions, conform to the RCM. We compare the composite data (i.e., the ensembles in the red staircases) for different values of surface impedance. These are shown in Fig. 12 for the real and imaginary parts of  $Z_{11}$  and  $Z_{12}$ .

To compare these with RCM predictions, we compute the variance of the impedance values for each histogram. According to the RCM, the variance of the histograms should satisfy

$$\text{Var}(R_{ij}) = \text{Var}(X_{ij}) = \frac{v_{ij}}{\pi\alpha} \quad (6)$$

where  $Z_{ij} = jX_{ij} + R_{ij}$  and

$$\alpha = \frac{k^2}{Q\Delta k^2} \quad (7)$$

is the dimensionless loss parameter,  $k = \omega/c$ ,  $A$  is the cavity area,  $Q$  is the cavity quality factor, and  $v_{11} = 1, v_{12} = 1/2$ . These relations follow from (2) in the  $\alpha \gg 1$  limit [12]. For the three loss values (80, 40, and 10  $\Omega$ ), we estimate the quality factors to be  $Q = 211, 422,$  and  $1690$ , respectively. These estimates were obtained by computing several eigenfunctions of the undriven cavity and averaging. The corresponding  $\alpha$ -values are 12, 6, and 1.5. The histograms shown in Fig. 12 confirm the trend that the variance decreases with increasing loss. We can be more quantitative by computing the variances and forming the quantity,  $\mu_{ij} = \frac{\pi\alpha}{2} [\text{Var}(R_{ij}) + \text{Var}(X_{ij})]$ , which should agree with  $v_{ij}$ . We note that the computed variances of the real and imaginary parts of the impedance elements for diagonal and off-diagonal elements are numerically very close, so in forming  $\mu_{ij}$  we average the variance of the real and imaginary parts. Table I shows the tabulation of the index  $\mu_{ij}$  giving the variance of the impedance values for diagonal,  $i = 1, j = 1$ , and off-diagonal,  $i = 1, j = 2$ , elements of the impedance matrix. The value is tabulated for three different surface impedance values. Also shown is the theoretical expectation based on (1) is shown.

Table I shows that the variances have the correct inverse dependence on the loss parameter. The coefficient  $\mu_{12}$  has close to the correct numerical value. However, the coefficient  $\mu_{11}$  is approximately a factor of 2 too large. The predicted values

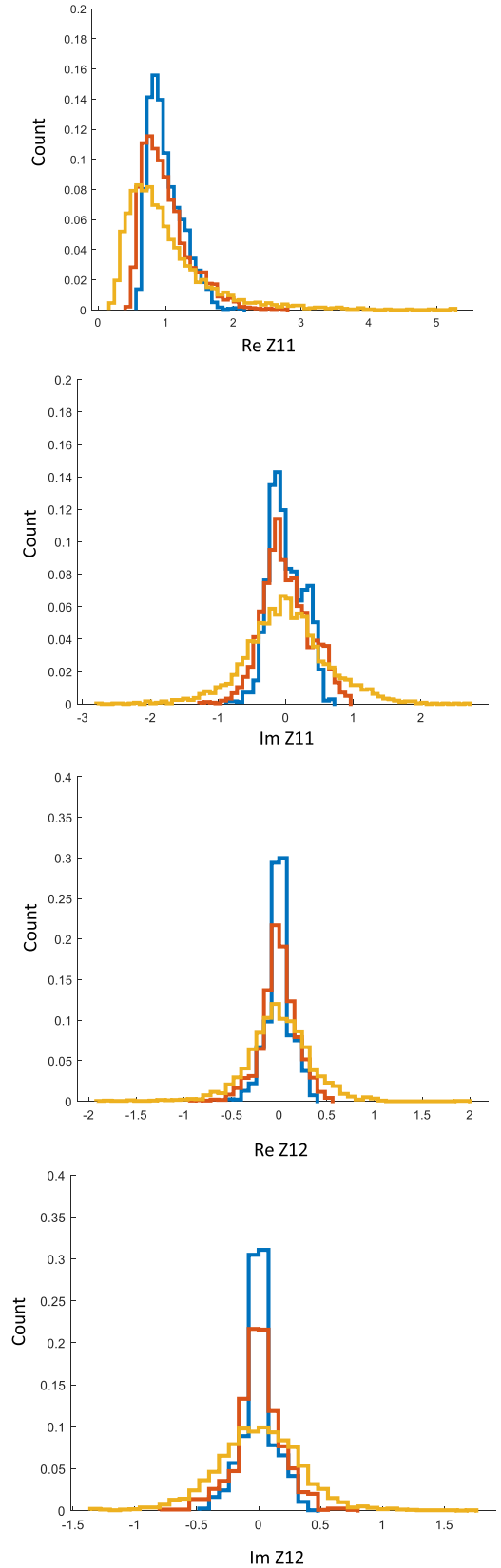


Fig. 12. Ensemble histograms of normalized impedance values (5) on the horizontal axes for various wall losses for the 110-mm aperture-like ports at 24–26 GHz. Colors correspond to loss values as follows: blue is for 80  $\Omega$ , red is for 40  $\Omega$ , and yellow is for 10  $\Omega$ . The labeled panels are as follows: (from top to bottom)  $\text{Re}\{Z_{11}\}$ ,  $\text{Im}\{Z_{11}\}$ ,  $\text{Re}\{Z_{12}\}$ , and  $\text{Im}\{Z_{12}\}$ .

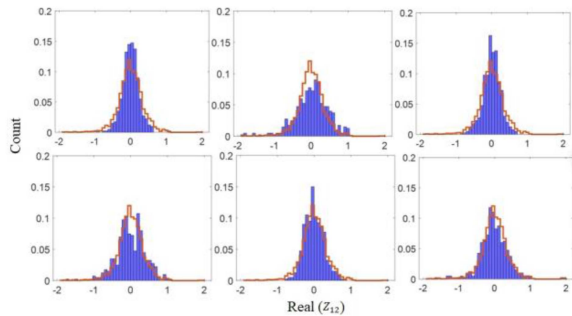


Fig. 13. Histogram plots for the normalized real ( $Z_{12}$ ) values (5) on the horizontal axes for six different scatterer positions. These histograms are for the 55-mm aperture-like sources at 24–26 GHz and  $40 \Omega$  loss. Blue bars show the real parts of  $Z_{12}$  for a particular position. The red staircase graph shows the histogram for the real values for all six scatterer positions combined.

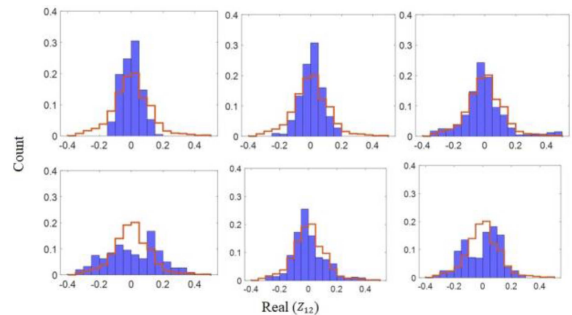


Fig. 14. Histogram plots for the normalized real ( $Z_{12}$ ) values (5) on the horizontal axes for six different scatterer positions. These histograms are for the 27.5-mm aperture-like sources at 24–26 GHz and  $40 \Omega$  loss. Blue bars show the real parts of  $Z_{12}$  for a particular position. The red staircase graph shows the histogram for the real values for all six scatterer positions combined.

TABLE II  
VARIANCES OF THE COMPOSITE HISTOGRAMS

$ij$	$v_{ij}$	$\mu_{ij}[110 \text{ mm}]$	$\mu_{ij}[55 \text{ mm}]$	$\mu_{ij}[27.5 \text{ mm}]$
11	1.0	2.35	1.96	1.823
12	0.5	0.68	0.26	0.29

are based on the assumption that the field is well represented by a superposition of uncorrelated modes. Here, we know that the main contributions to the impedance values come from the directive nature of the ports. Thus, it is perhaps not surprising that elements have larger than expected fluctuations.

We now fix the loss value at  $40 \Omega$  and vary the size of the aperture. Histogram data for aperture sizes of 55 mm and 27.5 mm are shown in Figs. 13 and 14. The individual realization histograms conform marginally to the composite histograms in these cases. According to the RCM, the aperture size should have no effect on the normalized impedance variances. Table II presents the variances of composite histograms for apertures of 110 mm, 55 mm, and 27.5 mm.

The variance of the diagonal element is roughly independent of aperture size as expected, but again a factor of two larger than expected from the RCM. The variance of the off-diagonal shows some dependence on aperture size, but no consistent trend.

The comparison of the composite histograms for various apertures is shown in Fig. 15. The composite histograms for

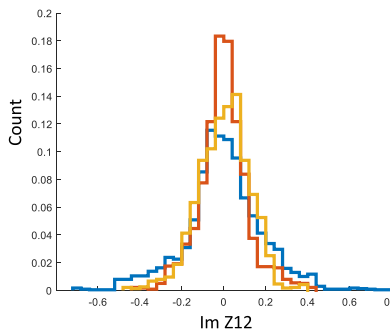
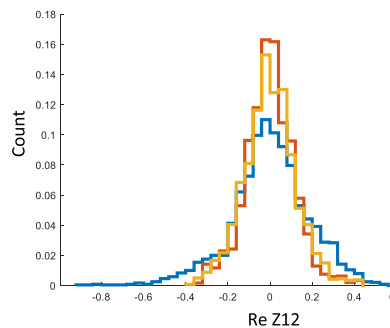
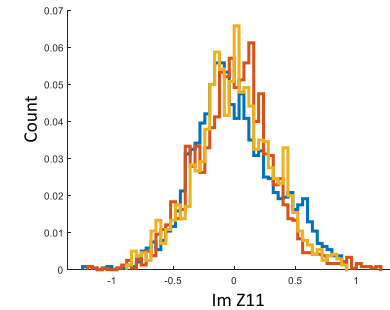
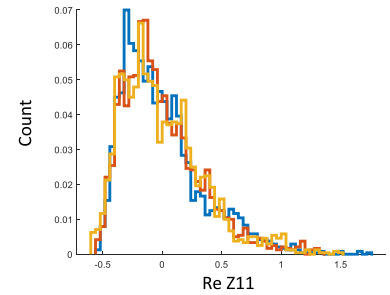


Fig. 15. Ensemble histograms of normalized impedance (5) for various aperture sizes at 24–26 GHz and  $40 \Omega$  loss. Blue bars are for 110-mm aperture, red bars are for 55-mm aperture, and yellow bars are for 27.5-mm aperture.

the diagonal elements are independent of aperture size, as expected. The composite histograms for the off-diagonal normalized impedance values show some variation with aperture size; primarily, the 110-mm aperture results show a greater range of fluctuations compared with the 55-mm and 27.5-mm aperture histograms.

## V. CONCLUSION

Wave scattering and coupling in a complicated geometry is a common challenge in many scientific fields because the complexity makes exact solutions impractical. On the other hand, wave chaos theories, such as RCM, offer useful approaches to

analyze the statistical properties of these complicated dynamical systems. In order to investigate the effect of a very directive energy source in wave chaotic cavities, we conducted full-wave solutions in HFSS of a bowtie cavity with a scatterer inside. We used aperture-like ports to inject EM energy into the cavity at 25 GHz. This was done to create a more directional beam, which we expected to create deviations from the random plane wave hypothesis—which is the basis of the RCM. We did find this to be true.

We first found that in a relatively high loss case ( $80 \Omega$  surface impedance), a directive port (110-mm aperture) produces impedance histograms that vary significantly from realization to realization. This is in contrast with the results of a nondirective port, for which the impedance histograms from different realizations were quite similar. We then varied the loss in the case of the directive port and found that as the loss was lowered, the histograms from different configurations became more similar. The loss rate for this transition was found to be consistent with the simple estimate that the emerging radiation beam would be wide enough to extend a distance equal to the cavity perimeter. Furthermore, the variance of the impedance values for different loss rates scaled with loss, as predicted by the RCM. However, there were numerical factors that differed consistently from RCM predictions. A general finding was that the fluctuations in impedance values were larger for diagonal elements as compared with off-diagonal elements.

Finally, we compared results from apertures of different sizes. The individual and composite histograms in these cases were similar. We computed the variances and again found that the diagonal elements had larger variances than expected on the basis of the RCM.

The calculations presented here are for a special case of modes in a quasi-2D cavity. A natural extension for future work would be the more extensive study of 3-D systems.

## REFERENCES

- [1] X. Li, C. Meng, Y. Liu, E. Schamiloglu, and S. D. Hemmady, "Experimental verification of a stochastic topology approach for high-power microwave effects," *IEEE Trans. Electromagn. Compat.*, vol. 57, no. 3, pp. 448–453, Jun. 2015.
- [2] M. Zhao, Y. Chen, X. Zhou, D. Zhang, and Y. Nie, "Investigation on falling and damage mechanisms of UAV illuminated by HPM pulses," *IEEE Trans. Electromagn. Compat.*, vol. 64, no. 5, pp. 1412–1422, Oct. 2022.
- [3] F. Adnan et al., "Wireless power distributions in multi-cavity systems at high frequencies," *Proc. Roy. Soc. A*, vol. 477, no. 2245, pp. 1–18, Jan. 2021.
- [4] B. Dietz, T. Guhr, H. L. Harney, and A. Richter, "Strength distributions and symmetry breaking in coupled microwave billiards," *Phys. Rev. Lett.*, vol. 96, no. 25, Jun. 2006, Art. no. 254101.
- [5] J. M. Jin, *The Finite Element Method in Electromagnetics*, 3rd ed. Hoboken, NJ, USA: Wiley, 2015.
- [6] A. Taflov and S. C. Hagness, *Computational Electrodynamics: The Finite Difference Time-Domain Method*. Boston, MA, USA: Artech House, 2005.
- [7] G. Tanner and N. Søndergaard, "Wave chaos in acoustics and elasticity," *J. Phys. A Math. Theor.*, vol. 40, no. 50, pp. 443–509, Nov. 2007.
- [8] R. Holland, *Statistical Electromagnetics*, 1st ed. Boca Raton, FL, USA: CRC Press, 1999.
- [9] M. Tang et al., "Ray dynamics and wave chaos in circular-side polygonal microcavities," *Phys. Rev. A*, vol. 99, no. 3, Mar. 2019, Art. no. 033814.
- [10] J. Gil Gil, Z. B. Drikas, T. D. Andreadis, and S. M. Anlage, "Prediction of induced voltages on ports in complex, three-dimensional enclosures with apertures, using the random coupling model," *IEEE Trans. Electromagn. Compat.*, vol. 58, no. 5, pp. 1535–1540, Oct. 2016.
- [11] X. Zheng, T. M. Antonsen, and E. Ott, "Statistics of impedance and scattering matrices of chaotic microwave cavities: Single channel case," *Electromagnetics*, vol. 26, no. 1, pp. 3–35, Aug. 2010.
- [12] X. Zheng, T. M. Antonsen, and E. Ott, "Statistics of impedance and scattering matrices of chaotic microwave cavities with multiple ports," *Electromagnetics*, vol. 26, no. 1, pp. 37–55, Aug. 2010.
- [13] S. Hemmady, T. M. Antonsen, E. Ott, and S. M. Anlage, "Statistical prediction and measurement of induced voltages on components within complicated enclosures: A wave-chaotic approach," *IEEE Trans. Electromagn. Compat.*, vol. 54, no. 4, pp. 758–771, Aug. 2012.
- [14] G. Gradoni, J. Yeh, B. Xiao, T. M. Antonsen, S. M. Anlage, and E. Ott, "Predicting the statistics of wave transport through chaotic cavities by the random coupling model: A review and recent progress," *Wave Motion*, vol. 51, no. 4, pp. 606–621, 2014.
- [15] M. L. Mehta, *Random Matrices*, 3rd ed. New York, NY, USA: Academic, 2004.
- [16] E. Ott, "Instability condition for confined waves with ergodic ray trajectories," *Phys. Fluids*, vol. 22, no. 11, pp. 2246, Nov. 1979.
- [17] M. V. Berry, "Chaotic behavior of deterministic systems," in *Proc. Les Houches Session*, Amsterdam, The Netherlands, 1983, pp. 171–271.
- [18] S. W. McDonald and A. N. Kaufman, "Spectrum and eigenfunctions for a Hamiltonian with stochastic trajectories," *Phys. Rev. Lett.*, vol. 42, no. 18, pp. 1189–1191, Apr. 1979.
- [19] D. A. Hill, "Plane wave integral representation for fields in reverberation chambers," *IEEE Trans. Electromagn. Compat.*, vol. 40, no. 3, pp. 209–217, Aug. 1998.
- [20] D-H. Wu, J. S. A. Bridgewater, A. Gokirmak, and S. M. Anlage, "Probability amplitude fluctuations in experimental wave chaotic eigenmodes with and without time reversal symmetry," *Phys. Rev. Lett.*, vol. 81, no. 14, pp. 2890–2893, Oct. 1998.
- [21] J. Hart, T. M. Antonsen, and E. Ott, "Effect of short ray trajectories on the scattering statistics of wave chaotic systems," *Phys. Rev. E*, vol. 80, no. 4, Oct. 2009, Art. no. 041109.
- [22] J. Yeh, J. Hart, E. Bradshaw, T. M. Antonsen, E. Ott, and S. M. Anlage, "Experimental examination of the effect of short ray trajectories in two-port wave-chaotic scattering systems," *Phys. Rev. E*, vol. 82, no. 4, Oct. 2010, Art. no. 041114.
- [23] H. Weyl, "Über die Gleichverteilung von Zahlen mod. Ein," *Math. Ann.*, vol. 77, pp. 313–352, 1916.
- [24] S. Hemmady, "A wave chaotic approach predicting and measuring electromagnetic field quantities of complicated enclosures," Ph.D. dissertation, Dept. Elect. Eng., Univ. Maryland, College Park, MD, USA, 2006.
- [25] J. Yeh, "Wave chaotic experiments and models for complicated wave scattering systems," Ph.D. dissertation, Dept. Elect. Eng., Univ. Maryland, College Park, MD, USA, 2013.



**Farasatul Adnan** received the B.S. degree in electrical engineering from the Ahsanullah University of Science & Technology, Dhaka, Bangladesh, in 2008, the M.S. degree in electrical engineering from McGill University, Montreal, QC, Canada, in 2011, and the Ph.D. degree in electrical engineering from the University of Maryland, College Park, MD, USA, in 2021.

During his master's, he worked in the field of computational electromagnetics, developing numerical methods to solve electromagnetic problems using the finite-element method. He was a Lecturer with Independent University, Bangladesh after his Masters. He worked with the Wave Chaos group and solved problems related to statistical electromagnetics during his Ph.D. In particular, he worked on developing novel methods for various aspects of the random coupling model using ray tracing and computational modeling. Since January 2022, he has been a Senior Bulk Acoustic Wave R&D Modeling Engineer with Qorvo, Inc., Apopka, FL, USA, where he has been working on developing resonator models for radio frequency (RF) filters for 5G RF front-end modules. His research interests include computational electromagnetics, statistical electromagnetics, mathematical modeling, and RF circuit design.



**Steven M. Anlage** (Member, IEEE) received the B.S. degree in physics from Rensselaer Polytechnic Institute, Troy, NY, USA, in 1982, and the M.S. and Ph.D. degrees in applied physics from the California Institute of Technology, Pasadena, CA, USA, in 1984 and 1988, respectively.

His graduate work concerned the physics and material properties of quasicrystals. His postdoctoral work with the Beasley–Geballe–Kapitulnik Group, Stanford University (1987–1990) concentrated on the high-frequency properties of high-temperature superconductors, including both basic physics and applications to tunable microwave devices. He is currently a Professor of physics and a Faculty Affiliate with the Department of Electrical and Computer Engineering and the Department of Materials Science and Engineering, University of Maryland, College Park, MD, USA. In 1990, he was appointed an Assistant Professor of physics in the Center for Superconductivity Research, University of Maryland, then an Associate Professor in 1997, and finally a Full Professor of physics in 2002. He was the interim Director of the Center for Nanophysics and Advanced Materials during 2007–2009 and is a member of the Maryland NanoCenter, where his research on high-frequency superconductivity has addressed questions of the pairing state symmetry of cuprate superconductors, the dynamics of conductivity fluctuations and vortices, and the fundamental electrodynamic properties of topological superconductors. His group was the first to realize the superconducting negative index of refraction metamaterials and has pioneered the development of superconducting quantum interference device (SQUID)-based metamaterials and the study of their properties. He has also developed and patented a near-field scanning microwave microscope for quantitative local measurements of electronic materials (dielectrics, semiconductors, metals, and superconductors) down to nanometer length scales. He and collaborators have developed a statistical prediction model for the effects of high-power microwave signals on electronics. He has also worked on time-reversed electromagnetics, examined the fundamental statistical properties of wave chaotic systems, explored the applications of machine learning to complex scattering systems, and developed the concept of complex time delay to reveal the underlying structure of the scattering matrix. In 2011, he was appointed as a Research Professor at the DFG-Center for Functional Nanostructures, Karlsruhe Institute of Technology, Karlsruhe, Germany. In 2019, he was appointed a Visiting Fellow at the Institute of Advanced Studies, Loughborough University, Loughborough, U.K. He has coauthored more than 200 research papers in scientific journals.

Dr. Anlage is a Member of the American Physical Society and the Materials Research Society. His research is supported by the National Science Foundation, the Department of Energy, and the US Department of Defense. He is an active consultant to the US Government.



**Thomas M. Antonsen Jr.** (Life Fellow, IEEE) received the bachelor's degree in electrical engineering and the master's and Ph.D. degrees from Cornell University, Ithaca, NY, USA, in 1973, 1976, and 1977, respectively.

During 1976–1977, he was a National Research Council Postdoctoral Fellow with the Naval Research Laboratory, and from 1977 to 1980, he was a Research Scientist with the Research Laboratory of Electronics, MIT. In 1980, he moved to the University of Maryland, College Park, MD, USA, where he joined the faculty of the Departments of Electrical Engineering and Physics in 1984. He is currently a Distinguished University Professor, a Professor of physics, and an Electrical and Computer Engineering Professor of electrophysics with the University of Maryland. He has held visiting appointments with the Institute for Theoretical Physics (U.C.S.B.), Isla Vista, CA, USA; the Ecole Polytechnique Federale de Lausanne, Lausanne, Switzerland; the University of Nottingham, Nottingham, U.K.; and the Institute de Physique Theorique, Ecole Polytechnique, Palaiseau, France. From 1998 to 2000, he was the Acting Director of the Institute for Plasma Research, University of Maryland. He has authored and coauthored more than 450 journal articles and coauthored the book *Principles of Free-Electron Lasers* (Chapman & Hall, 1992). His research interests include the theory of magnetically confined plasmas, the theory and design of high-power sources of coherent radiation, nonlinear dynamics in fluids, and the theory of the interaction of intense laser pulses and plasmas.

Dr. Antonsen was selected as a Fellow of the Division of Plasma Physics, American Physical Society, in 1986. In 1999, he was the co-recipient of the Robert L. Woods Award for Excellence in Vacuum Electronics Technology. He was the recipient of the IEEE Plasma Science and Applications Award in 2003, the Outstanding Faculty Research Award of the Clark School of Engineering in 2004, the IEEE J.R. Pierce Award for contributions to vacuum electronics in 2016, and the 2022 IEEE Marie Skłodowska-Curie Award. In 2010, he served as the Chair of the Division of Plasma Physics, American Physical Society. In 2017, he was elevated to the position of Distinguished University Professor. He has served on the editorial board of *Physical Review Letters*, *The Physics of Fluids*, and *Comments on Plasma Physics*.



**Edward Ott** (Life Fellow, IEEE) received the B.S. degree in electrical engineering from The Cooper Union, New York, NY, USA, in 1963, and the M.S. and Ph.D. degrees in electrophysics both from the Polytechnic Institute of Brooklyn, Brooklyn, NY, USA, in 1965 and 1967, respectively.

After receiving the Ph.D. degree, he was the National Science Foundation Postdoctoral Fellow with the Department of Applied Mathematics and Theoretical Physics, Cambridge University. Following his Postdoctoral research work, he was appointed as an Assistant Professor in the Department of Electrical Engineering, Cornell University, where he eventually became a Full Professor. In 1979, he moved from Cornell University to take up his current position as a Professor of physics and electrical engineering with the University of Maryland, College Park, MD, USA, where he is currently a Distinguished University Professor. His current research interest includes the area of chaos and nonlinear dynamics.